World Journal of Advanced Engineering Technology and Sciences
eISSN: 2582-8266
Cross Ref DOI: 10.30574/wjaets
Journal homepage: https://wjaets.com/

(RESEARCH ARTICLE)

Check for updates

Effect of the use of inorganic- based photoluminescent materials in solar energy devices application

Kimemia, D. Njoroge [1], Njoroge, W. K [1], Mwangi, I.W [2] and Tonui, M [3,*]

[1] *Department OF Physics, Kenyatta University, P.O BOX 43844 code 00100, Nairobi, Kenya.*
[2] *Department OF Chemistry, Kenyatta University, P.O BOX 43844 code 00100, Nairobi, Kenya.*
[3] *Department OF Chemistry, University of Kabianga, P.O. BOX 2030 code 20200, Kericho, Kenya.*

World Journal of Advanced Engineering Technology and Sciences, 2023, 09(02), 016–025

Publication history: Received on 17 May 2023; revised on 01 July 2023; accepted on 04 July 2023

Article DOI: https://doi.org/10.30574/wjaets.2023.9.2.0187

Abstract

The dynamic processes that take place in life require energy. The main convenient source of energy even in living tissue are hydrocarbons. This is due to the high-carbon based energy source that eventually converts fossil fuels. The preferred fuels as the primarily and industrial fuel contribute to the observed negative effects which emit pollutants to our environments and result to global warming. To mitigate such energy dependence, solar radiation has been exploited to produce clean energy through the use of photovoltaic cells. Nevertheless, natural radiation varies depending on the season of the year. This study investigated the properties of inorganic materials that support fluorescence after the source of light has been withdrawn. The minerals Sb/Ca/Mn/Ag were prepared hydrothermally to cultivate luminescent properties. The resulting products were characterized using Fourier Transformed Infrared (FTIR) spectroscopy and then applied to extend radiation in a photoactive material of a photocell. Optimal values of the prepared luminescent substance were established to produce the best generated potential in the fabricated solar cells when the natural radiation was withdrawn. Established receptive layer composites (KI/I_2: CX) were inserted into a molding dice on top of the photosensitive layer and joined together by pressing. The ensued inorganic luminescent cells optical characteristics were observed under UV radiation (320 - 400 nm) wavelength which produced sequential varying colorations from brown, light blue, blue to red before diminishing gradually as the incident radiation was removed. The open circuit potential voltage (V_{OC}) and current density (J_{SC}) generated parameters were observed. The (0.45, 0.4, and 0.086) V residue potential resulted due to shifting of IR by SbNO3, Sb-PO4, Sb-CO3 and Sb-O luminescent materials. The dopants had promising properties for radiation delay in photo voltaic devices application.

Keywords: Inorganic chemicals; Solar radiation; Delay; Photo luminescence; Absorption

1. Introduction

The excess use of fossils has resulted in global warming that has resulted leading to erratic climate change with erratic rainfall patterns and rapid evaporation of water from the soil. This makes life uncomfortable and a challenge to grow food crops or any other vegetation in most areas. To mitigate this, other options have to be exploited such as the use of solar radiation. This can be achieved by the use of renewable energy. This study reports on the fabrication of a cost effective and environmentally friendly solar cell using titanium dioxide to provide photovoltaic solar energy as an alternative energy source.

* Corresponding author: Tonui, M

Sequential progression of inorganic materials has actualized into notable evolution in photovoltaics. Their high performance and low-cost solution-based processes used for their preparation technology attest to their projected future utilization. Solar radiation is not constant at all times of the day and also differs depending on the season of the year. The net result is reduction in potential energy caused by such changes. Spectral losses in solar energy devices contribute to low responses and their achievable efficiencies. Direct dependence of normal solar irradiation using the existing solar dependent devices is thus affected. To increase their efficiency, spectral radiation need to be enhanced by use of materials which have potential to change the photo activity of some specific materials by altering their bang gaps. This happens due to introduction of defects in the material and shifts incident radiation, at a certain wavelength and emitted at a longer wavelength. That property was employed to extend supply of energy for a longer time constant after the source of natural radiation is withdrawn [1]. Reports by [2] noted that antimony and manganese doped calcium phosphors has the ability to transform ultraviolet radiations to delayed emission for a prolonged length of time. This enhances electroluminescence from milliseconds to several hours [2]. Calcium compounds which glow in minimum radiation forms double-activated crystal structures that accommodate Sb^{3+} ions and Mn^{2+} ions into their apatite lattice sites [2]. The radiation absorbed by Sb^{3+} ions in the crystal lattice is partly transferred to Mn^{2+} ions leading to high electroluminescence with a narrow band gap [1]. When illuminated with UV radiation, the impurities introduced energy levels which downshifted solar radiation in the energy gap between valance and conduction bands [3]. That downshifted radiation stimulated electrons towards the conduction band which were trapped into the d-donor levels for a while until they escaped to the valence band thus emitting lower energy photons [4].

Reports by [5,6] indicated that the absorbed energy is transferred to the neighboring luminescent impurities and emitted after a specific time of delay. According to [7], calcium, antimony, manganese and silver persistently glow after withdrawal of an incident radiation and thus find a large scientific application that require afterglow. Calcium and antimony compounds are widely applied to manufacture of battery anodes because they exhibit superior cycling stability with high charge retention capacity of 87.7 % [8]. A report by [3] noted that mixtures of the phosphor material at varying ratios yielded different afterglow durations.

[3] noted that the inorganic impurities with antimony and calcium compound introduced defects which alter the band gaps of the host materials [9]. This study considered the suitably of preparing antimony and calcium to accommodate manganese and silver ions to enhance radiation delay for an extended period after solar radiation diminishes.

1.1. The envisioned problem

The uneven irradiance resulted from natural sources experienced by solar radiation devices limits their expected performance in their times of operations [10]. Enhancing their capacity with varied band gap expand their absorption range bandwidth. That increase the length their desired optical radiation is made available to the host material due to fluorescence after the incident natural radiation is withdrawn and lengthen the duration needed for operation

2. Material and methods

The study applied experimental processes to analyze the organic photo luminescent material and the doped host material.

2.1. Chemicals and reagents

To obtain the fluorescent properties of the Sb/Mn/Ag doped calcium hydroxyapatite, the inorganic 0.22 g Sb, 12 g [$Ca(OH)_2$], 0.2 g (MnO_4) and 0.04 g of $AgNO_3$ were weighed into a (250 ml) beaker and 20 ml of dilute phosphoric acid (H_3PO_4) was added drop wise. To make Ag NPS, a solution of $AgNO_3$ dispersed in triethylamine was treated with a solution hydrazine. The solution was thoroughly stirred using a stirring rod as 10 ml of aqueous ammonium solution was added drop wise adjusting the pH of the system to 8. The stirring continued until a homogeneous phas1e was formed. The mixture was then placed into an oven at a temperature of 140 ^{0}C for 48 hours. The resultant was allowed to cool to room temperature then washed with acetone to remove ionic impurities to make it ready for use.

2.2. Instrumentation

All the material used in this study were characterized using a Shimadzu FTIR 2014 spectrometer. The schematic presentation of the equipment used is as shown in Figure1.

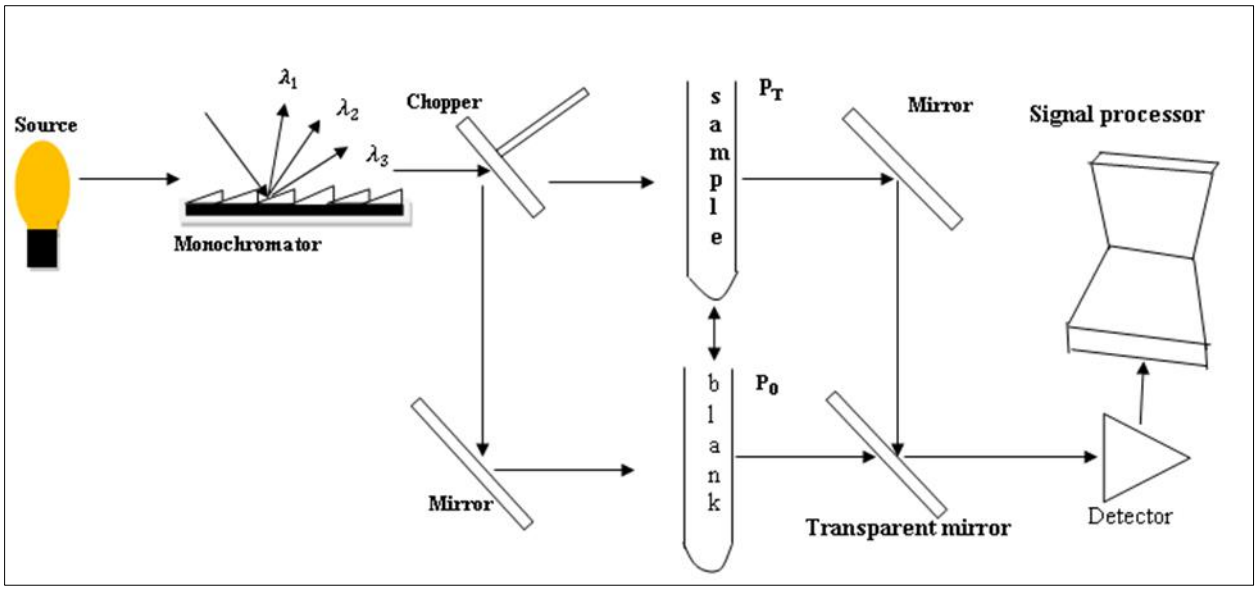

Figure 1 FTIR spectrometer (for IR absorption measurement)

The instrument consists of a source, interferometer, sample compartment, detector, amplifier, signal processor, and a computer. The source generates radiation which passes the sample through the interferometer and reaches the detector.

2.3. Fabrication of the cell doped with the different luminescent materials

This was achieved by taking (0.3) g TiO_2 finely ground photo active material mixed with varied masses of inorganic Sb/Ca/Mn/Ag material respectively in a molding dice and pressed at a constant pressure of 10000 psi. The anode layer preparation was done by molding with the pressing dice at constant (0.18/Cx) g mass ratios of I_2 KI/Cx mixture and disposed on the previously molded photo active disc. The resulted layers of the luminescent photo active cells were then carefully removed and placed on a conductor to enable measurement of their I-V characteristics. Figure 2 shows a schematic presentation of the luminescent solar cell.

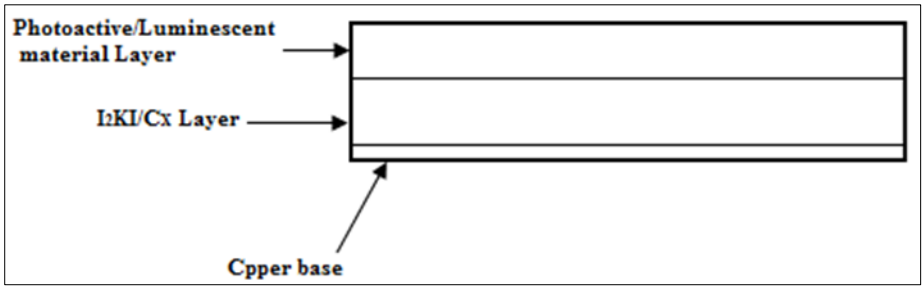

Figure 2 Sketch of the fabricated luminescent solar cell

2.4. I-V Characterization

The I-V characterization of the cells was carried out and the assembly for the experiment is as shown in Figure 3.

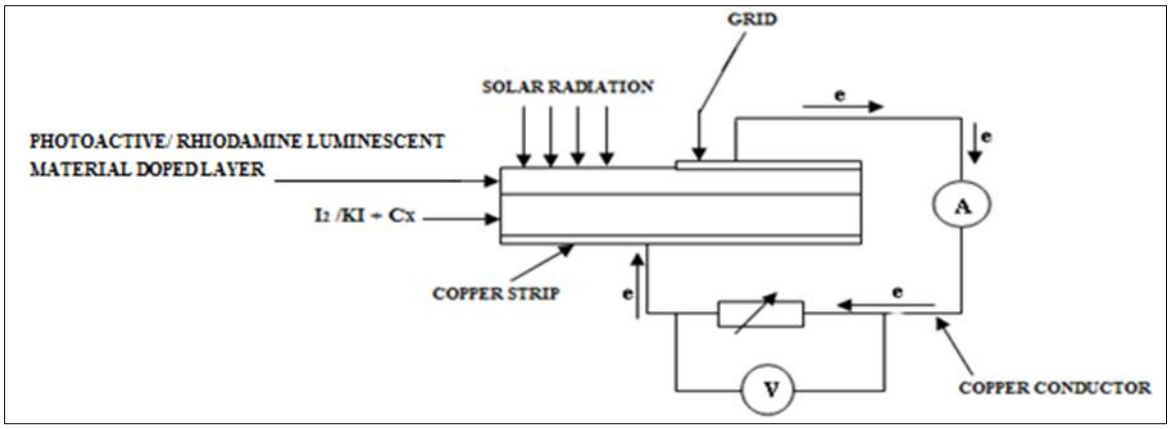

Figure 3 I-V Characterization Circuit for the fabricated solar cell

V-T Characterization

A stopwatch was incorporated besides the set to determine the time of potential decay when the set was transferred to a darkroom. Figure 4 shows the circuit diagram for the potential-time decay characterization.

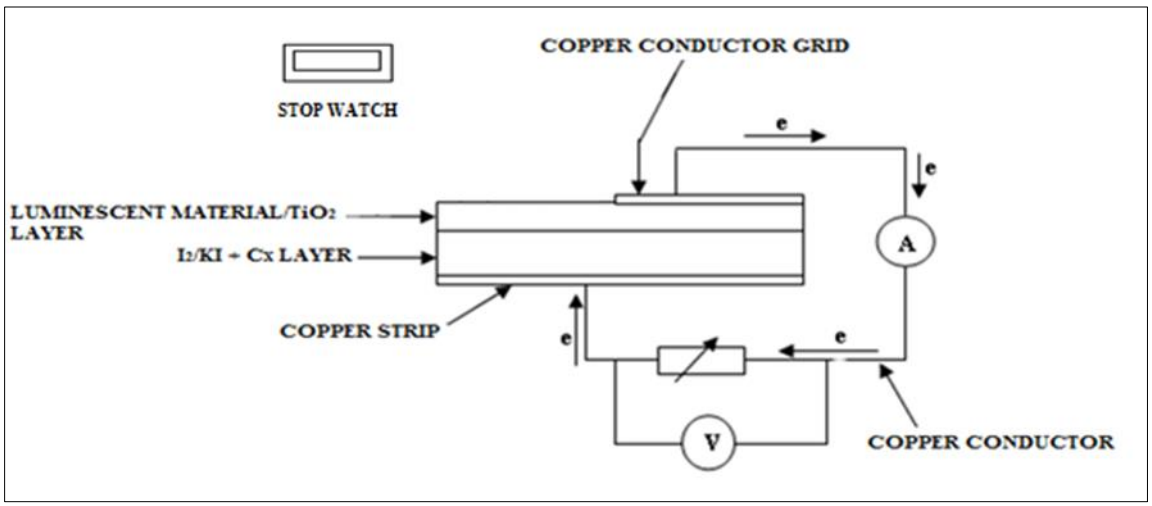

Figure 4 Potential Decay Characterization Circuit

The equations tabulated in Table 1 were applied to calculate the derived parameters of the luminescent solar cell.

Table 1 Expressions for calculating the derived parameters of the luminescent solar cell

Parameters to be Calculated
Maximum Power (P_{MAX}) = (J_{MP}) and (V_{MP})
Total radiant P_{IN} = 1000 W/m² = 100 mW/cm²
$\text{Fill Factor(FF)} = \frac{J_{MP} \times V_{MP}}{J_{SC} \times V_{OC}}$
Efficiency (η) = $\frac{V_{OC} \times I_{SC} \times FF}{P_{IN}}$

3. Results and discussion

The inorganic complex semiconductor-metal (sc/m) hybrid has nanostructure interface sheath with reduced electronic structure atoms forming defects with charge carriers traps dominated by varied Ag nanoparticles (NPs) and random physical interactions interfaces. The silver nanoparticles were made the *reduction of silver nitrate* by *hydrazine* hydrate in water ionic liquid micro emulsion. The resultant material was washed thoroughly with water the acetone. The absence of organic matter was confirmed using an FTIR spectrometer whose characteristics were as provided in Figure 5.

3.1. Chemical characterization of the inorganic (Sb/Ca/Mn/Ag) luminescent material

The dry Sb/Ca/Mn/Ag inorganic powder subjected to IR radiation generated by a Shimadzu FTIR 2014 spectrometer initiated a series of frequency bands shown in Figure 5.

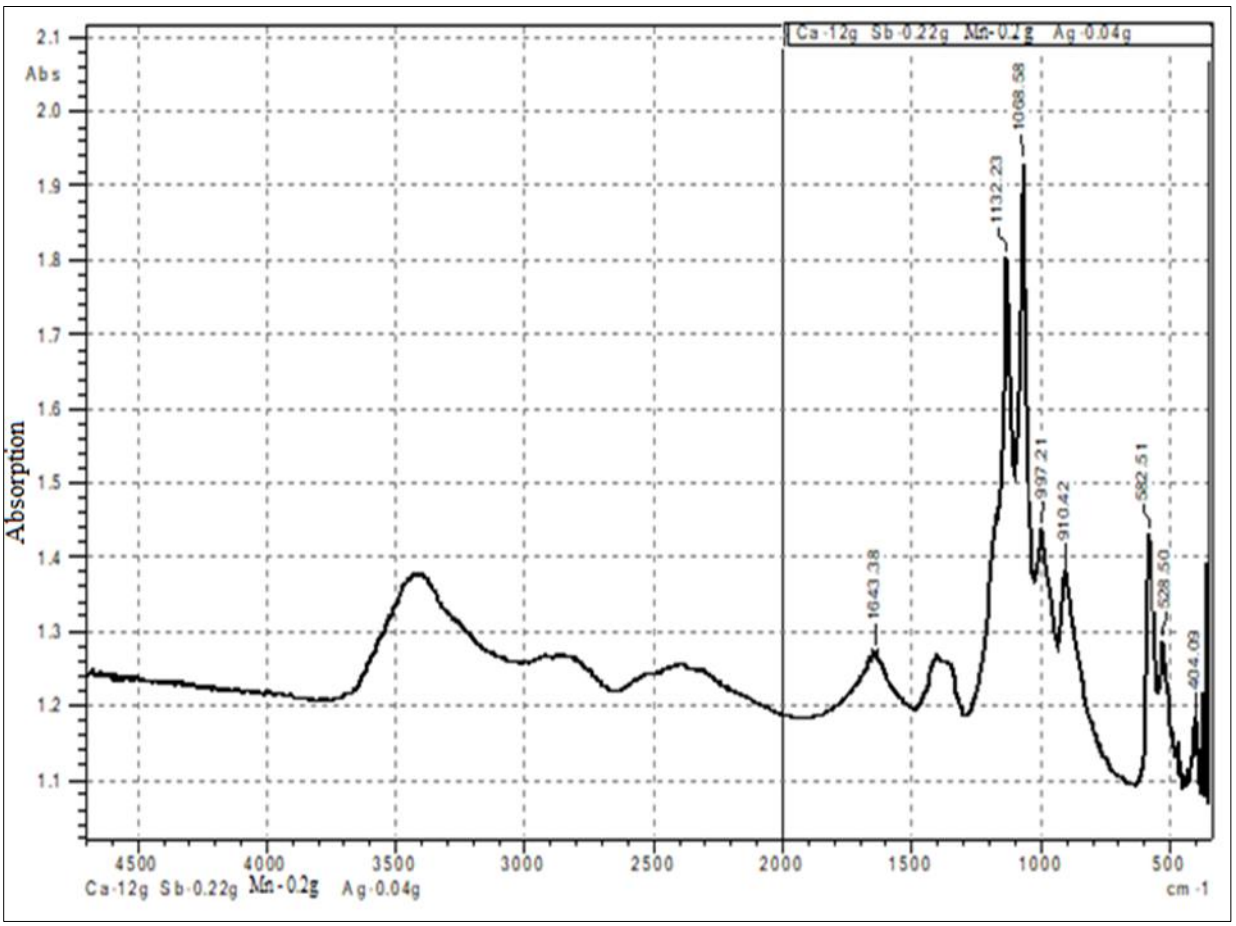

Figure 5 FTIR Absorption spectrum of the synthesized (Sb/Ca/Mn/Ag) luminescence material

Figure 5 shows a spectrum of Sb/Mn/Ag for the frequencies that were assigned to transfer of energy by Sb-NO_3, Sb-PO_4 and Sb-CO_3 and Sb-O centres. The signals of low intensity due to free nitrate ion were observed to resonate at 1356 - 828 cm^{-1} while that due to carbonate ion were observed at 1690 cm^{-1}.These results indicated that antimony bonding with different anions delayed radiations as evidenced by their respective resonant frequencies [11]. This is due to the splitting of d-orbitals groups resulting to d→d transitions which are relatively weak hence infrared active[11]. By extension, their results noted that varied colours resulted from delayed relaxation of excited electrons. Separate studies by [5,6] noted that different particle's momentum resulted to transfer of energy to the neighboring particles as illustrated by the following equations.

$$Ca^{2+} + hv \longrightarrow (Ca^{2+})^*$$
$$(Ca^{2+})^* + (Sb^{3+}) \longrightarrow Ca^{2+} + (Sb^{3+})^*$$
$$(Sb^{3+})^* + (Mn^{2+}) \longrightarrow (Sb^{3+}) + (Mn^{2+})^*$$
$$(Mn^{2+})^* + (Ag^{1+}) \longrightarrow (Mn^{2+}) + (Ag^{1+})^*$$
$$(Ag^{1+})^* \longrightarrow (Ag^{1+}) + hv$$

The equations show that there was energy transfer by the photo luminescent particles. That delayed relaxation was exploited in this study with a view to increase spectral traps in the $SbNO_3$, Sb-PO_4, Sb-CO_3 and Sb-O ions and released later to prolong interaction of radiation with the titanium dioxide (TiO_2) photo fluorescent material. A study of the delay in photo activity after withdrawal was carried out to investigate the potential delay by the doped TiO_2 solid solar cells.

3.2. Response of Sb/Ca/Mn/Ag luminescent materials luminescence material on radiation delay

Varying masses of inorganic (Sb/Mn/Ag) material were thoroughly mixed with separate (TiO_2) (1.00 g) mass photoactive material each as presented in Table 2.

Table 2 Materials composition of Sb/Ca/Mn/Ag -TiO_2 luminescent solar cells

Cell	Mass/g	
	Allicin Luminescent Material	TiO_2
Z1	0	1
Z2	0.01	1
Z_3	0.02	1
Z_4	0.03	1
Z_4	0.04	1
Z_5	0.05	1
Z_6	0.06	1

From the respective mixtures, seven photo active cells were fabricated and assigned labels (Z_1, Z_2, Z_3, Z_4, Z_5, Z_6, and Z_7). Receptive layers were made using (0.48 g) of graphite-iodine (Cx /I/KI) for each photo cell whose ratios were 0.3 g, 0.17 g and 0.01 g respectively.

3.2.1. Open circuit voltage (Potential) against Time Characterization of (inorganic Sb/Ca/Mn/Ag doped)-TiO_2

Fluorescent Solar Cells

The resulting cells were exposed to natural radiation and variation of potential was observed. The data obtained was presented in Table 3.

The cells were then transferred to a dark room and variation of potentials monitored for an interval of one hour was as shown in Table 4.

Table 3 I-V Characterization of (inorganic Sb/Ca/Mn/Ag doped)-TiO_2 luminescent solar cells at constant 0.25 g TiO_2

Potential /Volts	**Short Circuit Current(I_{SC})(mA) (±0.005)**						
	Z1	**Z2**	**Z3**	**Z4**	**Z5**	**Z6**	**Z7**
	(0 g)	**(0.01 g)**	**(0.02 g)**	**(0.03 g)**	**(0.04 g)**	**(0.05 g)**	**(0.06 g)**
0.381						0	
0.38					0	0.008	
0.378					0.008	0.018	0
0.377				0	0.009	0.022	0.006
0.361			0	0.006	0.018	0.045	0.015
0.352			0.004	0.01	0.02	0.05	0.019
0.349		0	0.009	0.013	0.023	0.053	0.021
0.332		0.006	0.014	0.019	0.027	0.059	0.027
0.307		0.01	0.017	0.024	0.032	0.066	0.031
0.266	0	0.014	0.021	0.029	0.034	0.071	0.037
0.243	0.016	0.018	0.026	0.033	0.036	0.072	0.041
0.193	0.029	0.023	0.026	0.036	0.039	0.076	0.048
0.135	0.041	0.029	0.033	0.044	0.046	0.082	0.058
0.125	0.043	0.03	0.034	0.045	0.049	0.084	0.059
0.111	0.047	0.031	0.035	0.047	0.051	0.086	0.0605
0.099	0.051	0.032	0.036	0.048	0.053	0.087	0.061
0.086	0.056	0.033	0.037	0.049	0.056	0.089	0.062
0.021	0.068	0.034	0.036	0.05	0.062	0.091	0.0625
0	0.075	0.035	0.038	0.051	0.066	0.095	0.063

Table 4 Potential(V_{OC}) against Time characteristic of the inorganic Sb/Ca/Mn/Ag doped – TiO_2) FCCs at 0.25 g TiO_2

Time/ Min	**Potential / Volts (±0.005)**						
	Z_1	**Z_2**	**Z_3**	**Z_4**	**Z_5**	**Z_6**	**Z_7**
	(0 g)	**(0.01 g)**	**(0.02 g)**	**(0.03 g)**	**(0.04 g)**	**(0.05 g)**	**(0.06 g)**
0	0.3	0.127	0.153	0.202	0.254	0.332	0.246
1	0.302	0.129	0.147	0.186	0.263	0.381	0.251
3	0.273	0.119	0.146	0.193	0.239	0.349	0.277
7	0.187	0.114	0.141	0.172	0.221	0.307	0.239
11	0.131	0.107	0.139	0.143	0.219	0.266	0.228
17	0.093	0.098	0.127	0.133	0.189	0.243	0.222
30	0.024	0.082	0.105	0.123	0.163	0.193	0.178
33		0.078	0.106	0.118	0.152	0.182	0.146
45		0.066	0.082	0.103	0.123	0.125	0.101
51		0.049	0.067	0.082	0.098	0.111	0.094
57		0.041	0.054	0.068	0.074	0.099	0.086
60				0.059	0.065	0.094	0.078

The results from Table 3 and 4 are presented graphically as shown in Figure 6 and 7 respectively.

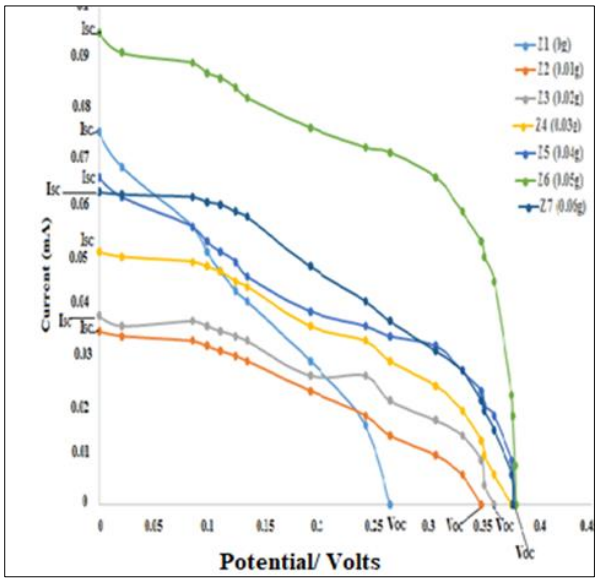

Figure 6 I-V characterization for (Sb/Ca/Mn*Ag) TiO_2 Fluorescent cells at constant (0.25 g) TiO_2

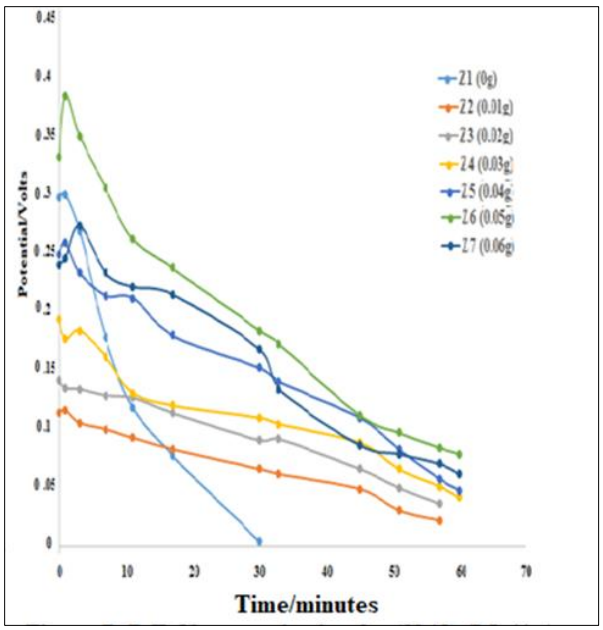

Figure 7 P-T characterization for (Sb/Ca/Mn*Ag) doped TiO_2 Fluorescent Solar cells at constant (0.25 g) TiO_2

Figure 6 shows I-V characteristics of first reducing (0.005, 0.004,0.02 and 0.01) mA charge rate surge as the generated voltage (potential) increased by (0.02) V due to (0.05, 0.04, 0.03 and 0.01) g mass variation of inorganic (Sb/Ca/Mn/Ag) dopant. A clipped charge signal (plateau clipped with a level of uniformity) occurred due to the significant (0.025 – 0.279) V potential change by (0.01, 0.02, 0.03 and 0.05) g dopant mass followed by irregular reducing charge rate between (0.015 -0.032) mA. The mass of (0.06) g displayed charge rate uniform plateau clipped at (0.099) V of the generated potential. The rest exhibited sections of graphically hyperbolic features or presentation of short circuit current as the as the potential increased to (0.266, 0.349, 0.361 and 0.377) V with the mass of (0.05) g generating the highest (0.381 V and 0.095 μA) (V_{OC}) and (I_{SC}) respectively. That resulted to (9.458 mW, 0.618 and 0.022 %) P_{MAX}, FF and PCE respectively. The buildup of charge rate was observed to be proportional to mass of the (Sb/Ca/Mn/Ag) dopants with varied potentials. However, cell (Z_1, (0 g)) void of (Sb/Ca/Mn/Ag) inorganic fluorescent material

generated the lowest (0.266 V) (V_{OC}) with (0.075) μA short circuit current with (0.305 and 6.085E-3%) FF and PCE respectively. This was attributed to the radiation due to the lack of enhancement for generation of high charge carrier density. The (FF and PCEs) derived parameters due to (0-0.06) g (Sb/Ca/Mn/Ag) fluorescent dopant resulted to {(0.372 and 4.544E-3 %), (0.484 and 6.639E-3 %) and (0.482 and 9.182E-3 %)}. This was attributed to the corresponding the quantity of *charge* per generated with time which is also referred to as charge rate density delivered to the external circuit. A study by [12] noted that fluorescent dopants mass ratios was proportional to the excited charge carriers density. Similar results reported by [13] indicated that dielectric constant of solvent material was proportional to the excited electron holes pairs density which determined the ensued ionic dissociation. Imbalance between dopant and the host material affected the potential with time delay which were the parameters of interest due to reduction of the intensity of excitation energy [14]. That enhancement further supported time delay in potential (voltage) as observed from Figure 7. The P-T characteristics in diminished radiation shows that (0.052, 0.065, 0.086, and 0.076 V) – (V_{OC}) delay resulted from {$Z_{4,b}$ (0.03) g, $Z_{5,b}$ (0.04) g, $6_{4,b}$ (0.05) g and $Z_{4,b}$ (0.06) g} fluorescent solar cells realized due to the (Sb/Ca/Mn/Ag-TiO_2) complex. Dielectric constant (*the property of a material to insulate)* of the dispersing TiO_2 host material was thought to be proportional to the resulted density electron holes pairs which determined the ensued ionic dissociation. A similar study by [12] reported that reduction in charge carriers density gave rise to instantaneous downturns of potential profiles. Imbalance between the dopant and perovskite species affected the parameters of interest resulting from the intensity of excitation energy [14]. The introduced signal was absorbed as {(Sb-NO_3) at $\lambda_{(1356-828)}$ cm^{-1}, (Sb-PO_4) at $\lambda_{(1402-1385)}$ cm^{-1}, (C-N) at $\lambda_{(1082)}$ cm^{-1}, (C-C) at $\lambda_{(1039)}$ cm^{-1}, (Sb-O) at $\lambda_{(1650-2100\ and\ 800-1000)}$ cm^{-1} as absorbed from the spectrum of Figure 5. The absorption peak shifted red to $\lambda_{(1593)}$ cm^{-1} and that at $\lambda_{(1353)}$ cm^{-1} shifted blue in the range $\lambda_{(1402-1385)}$ cm^{-1} for an antimony complex with the same anions. The band at $\lambda_{(460-448)}$ cm^{-1} and $\lambda_{(434-426)}$ cm^{-1} were attributed to Sb-O transferring energy to Mn centres. These results were verified when the antimony ions bonded to different anions was subjected to U-Vis in a darkroom as they resulted to delayed emissions with varied observed colours. That concurred with findings of [15] noted that absorption peaks of the ligands of C–N and C–C ionic bonds appeared at 1082 and 1039 cm^{-1} respectively. According to [16,17] the bands between 1650-2100 and 800-1000 cm^{-1} were due to (Sb–O) ionic bond while that between 1250 - 1650 cm^{-1} was contributed by the phosphate ion. [11] reported that splitting of d-orbitals groups differed in energy resulting to d→d orbital transitions which are relatively weak hence IR active that is it resonated with the infra-red region. Reports by [11] noted that varied colours result from delayed relaxation of excited electrons. That difference in wavelength occurred due symmetric and asymmetric stretching bonds of oxygen atoms coordinating with metallic ions monodentate and bidentate bridges modes, within the crystal structure in the complex [18].

4. Conclusion

The study observed that the inorganic luminescent material transferred energy to the neighboring species resulting to radiation delay by Ca^{2+}, Sb^{2+}, Mn^{2+} and Ag^{+} ions due to existence radiation after withdrawal of the spectral radiation. The defect traps were introduced by the doping material which resonated at 1356 - 828 cm^{-1} while that due to carbonate ion resonated at 1690 cm^{-1}. The absorbed infrared radiation was shifted to longer wavelengths (1593, 1353, 1402, and 1385) cm^{-1} by the complex with the respective anions. The band at (460 – 448) cm^{-1} and 434 - 426 cm^{-1} were due to Sb-O transferring energy to Mn centres. These results indicated that antimony ionic bonding with different anions contributed to delayed radiations as evidenced with their respective resonant frequencies emitting varied colours. The ligands of C–N and C–C ionic bonds were observed to resonate at 1082 and 1039 cm^{-1} respectively. That down conversion (to lower energy) gave rise to potential delay of 0.086V. The inorganic dopants had promising properties for radiation delay in photo voltaic devices application.

Compliance with ethical standards

Acknowledgments

A lot of gratitude to Dr. Jane Mburu, Chemistry Department, Kenyatta University, for her support with inorganic luminescent materials synthesis equipment and space and their chemical characterization. My sincere appreciation to Mr. Fred Mundimba of Physics department, Kenyatta University, for the P - T and I-V instruments he accorded to me.

Disclosure of conflict of interest

Authors declare their sincere lack of knowledge of any known competing financial or personal relationships that could have appeared to influence the work reported in this research article.

References

[1] McArthur EA, Morris-Cohen AJ, Knowles KE, Weiss EA. Charge carrier resolved relaxation of the first excitonic state in CdSe quantum dots probed with near-infrared transient absorption spectroscopy. The Journal of Physical Chemistry B. 2010, 114(45):14514–20.

[2] Qu B, Zhang B, Wang L, Zhou R, Zeng XC. Mechanistic study of the persistent luminescence of CaAl2O4: Eu, Nd. Chemistry of Materials. 2015, 27(6):2195–202.

[3] Yang X, Yan D. Strongly Enhanced Long-Lived Persistent Room Temperature Phosphorescence Based on the Formation of Metal–Organic Hybrids. Advanced Optical Materials. 2016, 4(6).

[4] Dorenbos P. Charge transfer bands in optical materials and related defect level location. Optical Materials. 2017, 69:8–22.

[5] Schwede J, Bargatin I, Riley D, materials BHN, 2010 undefined. Photon-enhanced thermionic emission for solar concentrator systems. nature.com. 2010, 9.

[6] Tummeltshammer C, Taylor A, Kenyon AJ, Papakonstantinou I. Losses in luminescent solar concentrators unveiled. Solar Energy Materials and Solar Cells. 2016 Jan 9, 144:40–7.

[7] Truccolo G, Boseley R, Lewis S, Physics WGH on the, 2020 undefined. Forensic applications of rare earths: Anticounterfeiting materials and latent fingerprint developers. Elsevier.

[8] Liu X, Du Y, Xu X, Zhou X, … ZDTJ of P, 2016 undefined. Enhancing the anode performance of antimony through nitrogen-doped carbon and carbon nanotubes. ACS Publications.

[9] Li W, Long R, Tang J, Prezhdo O V. Influence of Defects on Excited-State Dynamics in Lead Halide Perovskites: Time-Domain ab Initio Studies. Journal of Physical Chemistry Letters. 2019 Jul 5, 10(13):3788–804.

[10] Al-Alwani MA, Mohamad AB, Ludin NA, Kadhum AAH, Sopian K. Dye-sensitised solar cells: Development, structure, operation principles, electron kinetics, characterisation, synthesis materials and natural photosensitisers. Renewable and Sustainable Energy Reviews. 2016, 65:183–213.

[11] McNicholas BJ, Grubbs RH, Winkler JR, Gray HB, Despagnet-Ayoub E. Tuning the formal potential of ferrocyanide over a 2.1 V range. Chemical Science. 2019, 10(12):3623–6.

[12] Ruiz-Jorge F, Portela J, Sciences JSOA, 2020 undefined. Synthesis of micro-and nanoparticles in sub-and supercritical water: from the laboratory to larger scales. mdpi.com. 2020 Aug 1, 10(16).

[13] Quan LN, Kang J, Ning CZ, Yang P. Nanowires for photonics. Chemical reviews. 2019, 119(15):9153–69.

[14] Singh O, Agrawal A, Selvaraj T, Ghosh IK, Vempatapu BP, Viswanathan B, et al. Renewable Aromatics from Tree-Borne Oils over Zeolite Catalysts Promoted by Transition Metals. ACS Applied Materials and Interfaces. 2020 Jun 3, 12(22):24756–66.

[15] Olajire AA, Ifediora NF, Bello MD, Benson NU. Green synthesis of copper nanoparticles using Alchornea laxiflora leaf extract and their catalytic application for oxidative desulphurization of model oil. Iranian Journal of Science and Technology, Transactions A: Science. 2018, 42:1935–46.

[16] Kaviyarasu K, Sajan D, Devarajan PA. A rapid and versatile method for solvothermal synthesis of Sb2O3 nanocrystals under mild conditions. Applied Nanoscience (Switzerland). 2013 Dec 1, 3(6):529–33.

[17] Nahyoon NA, Liu L, Rabé K, Nahyoon SA, Abro AH, Yang F. Efficient degradation of rhodamine B with sustainable electricity generation in a photocatalytic fuel cell using visible light Ag3PO4/Fe/GTiP photoanode and ZnIn2S4 photocathode. Journal of the Taiwan Institute of Chemical Engineers. 2019, 96:137–47.

[18] Liu T, Yang RG, Zhong GQ. Synthesis, structural characterization, and antibacterial activity of novel erbium (III) complex containing antimony. Bioinorganic Chemistry and Applications. 2018, 2018.